

## Electronic superlattices in corrugated graphene

A. Isacsson,<sup>1,\*</sup> L. M. Jonsson,<sup>1</sup> J. M. Kinaret,<sup>1</sup> and M. Jonson<sup>2,3</sup>

<sup>1</sup>Department of Applied Physics, Chalmers University of Technology, SE-412 96 Göteborg, Sweden

<sup>2</sup>Department of Physics, Göteborg University, SE-412 96 Göteborg, Sweden

<sup>3</sup>School of Engineering and Physical Sciences, Heriot-Watt University, Edinburgh EH14 4AS, Scotland, United Kingdom

(Received 13 December 2007; published 22 January 2008)

We theoretically investigate electron transport through corrugated graphene ribbons and show how the ribbon curvature leads to an electronic superlattice with a period set by the corrugation wavelength. Transport through the ribbon depends sensitively on the superlattice band structure which, in turn, strongly depends on the geometry of the deformed sheet. In particular, we find that for ribbon widths where the transverse level separation is comparable to the band edge energy, a strong current switching occurs as a function of an applied back gate voltage. Thus, artificially corrugated graphene sheets or ribbons can be used for the study of Dirac fermions in periodic potentials. Furthermore, this provides an additional design degree of freedom for graphene-based electronics.

DOI: 10.1103/PhysRevB.77.035423

PACS number(s): 73.50.Td, 73.21.Cd, 73.23.-b

### I. INTRODUCTION

A single layer of graphite, known as graphene, was studied for the first time experimentally in 2004.<sup>1</sup> This started a massive interest in graphene, mainly because it is a two-dimensional gapless semiconductor with massless “relativistic” quasiparticles.<sup>2–8</sup> An unusual integer quantum Hall effect<sup>9,10</sup> and a predicted minimal conductivity  $\sigma = 4e^2/(h\pi)$  are among the manifestations of the linear energy dispersion in the vicinity of the Fermi energy. In addition to being a tool for studying fundamental physics, graphene is also of interest for device applications [e.g., transistors, lenses, and nanoelectromechanical system (NEMS) resonators<sup>11–14</sup>]. For a review on the electronic properties of graphene, see Ref. 15.

Proposed graphene-based devices typically rely on external electrostatic gates for controlling the electronic transport. In this paper, however, we show that the effective potential induced in a graphene ribbon placed on a corrugated substrate can strongly alter the transport properties of graphene. This effective potential is determined by the local curvature<sup>16</sup> of the ribbon and introduces an additional design degree of freedom of interest for both fundamental studies of graphene and graphene-based electronic devices. The corrugation also leads to an induced gauge field that has been studied by other authors.<sup>17,18</sup> For illustration, we focus here on periodically modulated surfaces—superlattices—and show how the corresponding band structure can be readily probed by conductance measurements.

### II. MODEL

We consider a single graphene ribbon placed on a corrugated surface and biased by a small dc voltage, as shown in Fig. 1. In the tight binding description, the ribbon is described by

$$\hat{H}_{\text{TB}} = \sum_{\langle i,j \rangle} t_{ij} a_i^\dagger b_j + \sum_{\langle\langle i,j \rangle\rangle} t'_{ij} (a_i^\dagger a_j + b_i^\dagger b_j) + \text{H.c.} \quad (1)$$

Here,  $\langle i,j \rangle$  denote nearest neighbors ( $a$  and  $b$  refer to atoms on different sublattices) and  $\langle\langle i,j \rangle\rangle$  next nearest neighbors.

When the ribbon is deformed, the matrix elements  $t$  and  $t'$  change. Thus, if  $t_{ij} = V_{pp\pi}$  describes hopping between atoms  $i$  and  $j$  on a flat graphene sheet, we find (details are given in the Appendix) that for a deformed sheet,<sup>16,19</sup>  $t_{ij}^{(')}$  is replaced by

$$\tilde{t}_{ij}^{(')} = \frac{u_{ij}^2}{d_{ij}^4} [(V_{pp\sigma} - V_{pp\pi})(\mathbf{n}_i \cdot \mathbf{d}_{ij})(\mathbf{n}_j \cdot \mathbf{d}_{ij}) + V_{pp\pi} d_{ij}^2 \mathbf{n}_i \cdot \mathbf{n}_j].$$

Here,  $\mathbf{u}_{ij}$  is the vector connecting atoms  $i$  and  $j$  in the undeformed lattice while  $\mathbf{d}_{ij}$  is the corresponding vector after deformation. The surface normals are denoted by  $\mathbf{n}_{i(j)}$ . While a general deformation involves both bending and stretching, we will restrict our attention here to pure bending deformations in one direction, i.e.,  $z = h(x)$  (see Fig. 1). We write the new matrix elements  $\tilde{t}_{ij}^{(')} = t_{ij}^{(')} + \delta_{ij}^{(')}$ , and to second order in  $\partial_x^2 h$ , we find

$$\delta_{ij}^{(')} = - \frac{(\partial_x^2 h)^2 (\mathbf{u}_{ij} \cdot \hat{x})^4}{2u_{ij}^2} \left[ \left( \frac{u_{ij}^2}{(\mathbf{u}_{ij} \cdot \hat{x})^2} - \frac{2}{3} \right) V_{pp\pi} + \frac{1}{2} V_{pp\sigma} \right].$$

Inserting the new matrix elements in Eq. (1) and expanding around the Fermi points  $\mathbf{K}$  and  $\mathbf{K}'$  results in an effective Hamiltonian with two new terms  $\mathbf{A}_{\text{eff}}$  and  $\Phi_{\text{eff}}$ , which are of order  $a_0^2 (\partial_x^2 h)^2$  ( $a_0 = 1.42 \text{ \AA}$  is the lattice constant). For electrons near the  $\mathbf{K}$  point, the Hamiltonian is

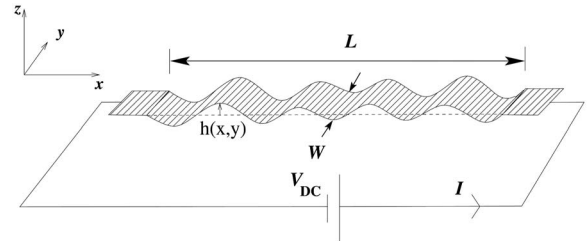


FIG. 1. Schematic illustration of the graphene ribbon system investigated in this paper. The dc-biased ribbon of width  $W$  rests on a corrugated substrate surface of length  $L$  and height profile  $h(x,y)$ .

$$\hat{H}_{\text{eff}} = \hbar v_F \hat{\sigma} \cdot [-i \nabla + \mathbf{A}_{\text{eff}}(\mathbf{x})] + eV_G + \Phi_{\text{eff}}(\mathbf{x}). \quad (2)$$

Here,  $\hat{\sigma} = \hat{x}\sigma_x + \hat{y}\sigma_y$  and  $\sigma_{x,(y)}$  are Pauli matrices,  $v_F = 10^6$  m/s is the Fermi velocity, and  $eV_G$  can be produced by the action of a back gate.

Unless time reversal symmetry is broken, e.g., by a magnetic field, the effective vector potential  $\mathbf{A}_{\text{eff}}(\mathbf{x})$  at the  $\mathbf{K}$  point and its time reversed counterpart at the  $\mathbf{K}'$  point only contribute to second order in  $a_0^2(\partial_x^2 h)^2$  and will be ignored in what follows. The second new term corresponds to an effective potential, which, for graphene bent along the ‘‘armchair’’ direction, is

$$\Phi_{\text{eff}}(x) = \frac{27}{4} a_0^2 (\partial_x^2 h)^2 \left( \frac{3}{8} V_{pp\sigma}^{(aa)} - \frac{1}{6} V_{pp\pi}^{(aa)} \right).$$

In addition, because of the vanishing of the first order matrix element of  $\mathbf{A}_{\text{eff}}(\mathbf{x})$ , a third new term corresponding to a local variation in Fermi velocity should be considered. However, for long wavelengths,  $ka_0 \ll 1$ , this term can be shown to be much smaller than the effective potential  $\Phi_{\text{eff}}$ .

The form of the effective potential is simplified if we take the shape of the ribbon to be  $h(x,y) = A \sin(n\pi x/L)$ . This approximation captures the qualitative behavior of a general periodic potential and results in the expression (see the Appendix)

$$\Phi_{\text{eff}}(x) = E_0 (A/a_0)^2 (k_s a_0)^4 (1 - \cos k_s x), \quad (3)$$

where  $k_s = 2n\pi/L$  and  $E_0 \approx 0.22$  eV. Note that  $\Phi_{\text{eff}}(x)$  is positive definite (repulsive), and its strength varies rapidly with  $k_s$  due to the factor  $(k_s a_0)^4$ . Because we have assumed  $k_s a_0 < 1$ , large amplitudes  $A/a_0 \gg 1$  are necessary. Hence, it is important that Eq. (3) is transformed to a coordinate system  $s = s(x)$  that follows the graphene ribbon. The relation between  $s(x)$  and  $x$  is

$$s(x) = \frac{L}{\pi n} \sqrt{1 + \tilde{A}^2} E \left( \frac{n\pi x}{L}, \sqrt{\frac{\tilde{A}^2}{1 + \tilde{A}^2}} \right),$$

where  $E$  is the elliptic integral of the second kind and  $\tilde{A} = n\pi A/L$ . The total length of the graphene sheet is then  $s(L)$ . For simplicity, we will from hereon write  $x$  rather than  $s(x)$  for the coordinate along the sheet.

For narrow graphene nanoribbons, the choice of transverse electronic boundary conditions is of great importance. They depend on the configuration of carbon atoms along the edge<sup>20</sup> as well as the ribbon width. In this paper, we use boundary conditions for a metallic armchair edge. The wave vector quantization in the transverse direction ( $y$ ) gives  $k_n = n\pi/W$ . In the absence of fields, the wave functions satisfy the Dirac equation

$$-i\hbar v_F \begin{bmatrix} \nabla \cdot \hat{\sigma} & 0 \\ 0 & \nabla \cdot \hat{\sigma}^* \end{bmatrix} e^{ik_x} \phi_n^\pm(k,y) = \epsilon_n^\pm e^{ik_x} \phi_n^\pm(k,y),$$

with  $\epsilon_n^\pm = \pm \hbar v_F \sqrt{k^2 + k_n^2}$ . For  $n > 0$ , the eigenspinors are

$$\phi_n^\pm(k,y) = e^{ik_n y} \begin{pmatrix} 1 \\ \pm e^{i\phi_n(k)} \\ \pm e^{i\phi_n(k)} \\ 1 \end{pmatrix} + e^{-ik_n y} \begin{pmatrix} \pm e^{i\phi_n(k)} \\ 1 \\ 1 \\ \pm e^{i\phi_n(k)} \end{pmatrix},$$

which are twofold degenerate and for  $n=0$ , they are

$$\phi_0^\pm(k,y) = [1, \pm \text{sgn}(k), 1, \pm \text{sgn}(k)]^T$$

and nondegenerate. The factors  $\exp(i\phi_n(k)) = (k + ik_n) / \sqrt{k^2 + k_n^2}$  correspond to the incidence angle of the electrons.

In the presence of a scalar potential that only depends on  $x$ , there can be no band mixing although positive and negative energy solutions belonging to the same band may mix. Thus, we look for solutions of the form

$$\psi_n(x,y) = \int dk \gamma_n^+(k) [\phi_n^+(k,y) + \phi_n^-(k,y)] e^{ikx} + \int dk \gamma_n^-(k) [\phi_n^+(k,y) - \phi_n^-(k,y)] e^{i[kx - \phi_n(k)]},$$

which, together with Eq. (2), leads to the equation

$$[-i\hbar v_F (\partial_x \sigma_x + ik_n \sigma_y) + V(x)] \bar{\gamma}_n(x) = \epsilon \bar{\gamma}_n(x) \quad (4)$$

for the two-component spinor  $\bar{\gamma}_n(x) = [\gamma_n^+(x), \gamma_n^-(x)]$  with  $V(x) = eV_G + \Phi_{\text{eff}}$ .

### III. TRANSPORT IN CORRUGATED GRAPHENE

Before analyzing the curvature effects, we begin with a general discussion of the band structure for periodic potentials in the Dirac equation (see also Refs. 21 and 22). For this, we consider an infinite graphene strip of width  $W$  subject to the periodic potential  $V(x) = V_0 \sin(2\pi x/\lambda)$ . In this case, Eq. (4) can be solved numerically and the resulting band structure in the reduced zone scheme is shown in the left panel of Fig. 2. The right panel shows the number of conducting channels as a function of energy and one sees that the periodic potential produces pseudogaps whenever this number has a minimum. It is interesting to note that the gap sizes increase with band index  $n$ . This is consistent with our knowledge of the Klein tunneling since a potential barrier has no effect on massless relativistic particles, while for finite mass, there is an effect which increases with mass.<sup>23</sup> Here we consider one-dimensional motion along the graphene ribbon in bands corresponding to quantized transverse momenta  $k_n$ . In the effective equation for the longitudinal motion [Eq. (4)], these transverse momenta produce a mass term that is zero for  $n=0$  and finite and increasing with  $n$  for  $n > 0$ .

The band structure in Fig. 2 can be probed by transport measurements. To demonstrate this, we adopt a Landauer approach together with a transfer matrix method and calculate the transmission probabilities assuming coherent and ballistic transport. The conductance is then found from  $G = (4e^2/h) \sum_n t_n$ , where  $t_n$  is the transmission probability for channel  $n$  and the sum over  $n$  runs over all channels. The

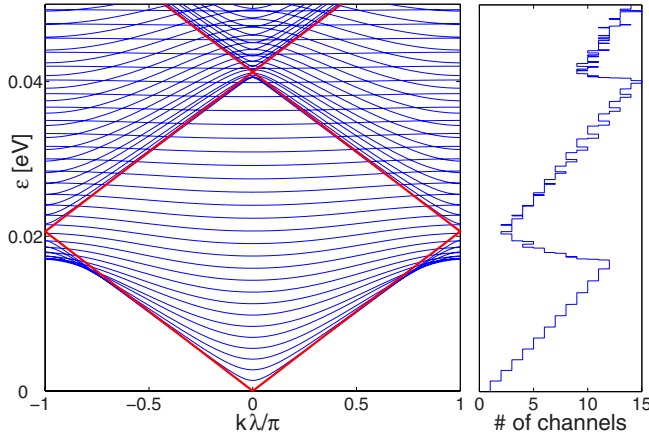


FIG. 2. (Color online) Band structure for an infinitely long and  $1 \mu\text{m}$  wide metallic graphene sheet with armchair edges subjected to a periodic potential  $V_0 \sin(2\pi x/\lambda)$  ( $V_0 \sim 2.5 \text{ meV}$ ) (left panel) and the corresponding number of bands crossing each energy (right panel). The linear band calculated for  $k_n=0$  (bold line) is not distorted by the periodic potential, which is a manifestation of the Klein paradox. A pseudogap is visible for  $E \sim 0.02 \text{ eV}$  and another at  $E \sim 0.04 \text{ eV}$  roughly corresponding to the free electron energies at  $k=\pi\lambda$  and  $k=2\pi\lambda$ . The band structure is in this case symmetric for positive and negative energies (not shown).

transmission probabilities  $t_n$  are obtained from<sup>24</sup> the transfer matrices  $T_n = \prod_{m=1}^N T_n^{(m)}$ . Here, the interval  $0 < x < s(L)$  is divided into  $N$  steps each having a constant potential  $V_m = V(x_m)$ ,  $x_m = ms(L)/N$ . The transfer matrices between slices are found from the requirement that the wave functions be continuous everywhere (current conservation). The reservoirs on the left and right sides are taken to be infinitely wide graphene strips. As will be seen, this gives rise to a Fabry-Pérot-like interference pattern in the conductance, due to reflections at the reservoir-ribbon interfaces, as the backgate voltage is varied. These fluctuations are expected to smear out at finite temperatures and in the presence of impurities. As pointed out in Ref. 25, it is in general not allowed (as in the case of a two-dimensional electron gas) to introduce a general adiabatic widening of the strip to remove these fluctuations. Such a widening will introduce a changing structure of the transverse boundary conditions and a detailed description of the edge geometry is necessary.

The conductivity of a finite system of length  $L=1 \mu\text{m}$  is shown as a function of gate voltage and strip width in Fig. 3. For widths  $W > L \gg \lambda$ , the conductivity does not change appreciably as the ribbon becomes wider, whereas for narrow strips, strong alteration of the conductivity occurs. The inset shows the conductivity for parameters corresponding to Fig. 2. The conductivity minima agree with the predicted pseudogaps from the infinite structure in Fig. 2.

Now, we consider a finite length graphene ribbon placed on a corrugated substrate. We will specifically consider narrow strips where the transverse energy level spacing  $\Delta\epsilon_n \sim \hbar v_F/W$  is of the same order as the band edge energy, i.e.,  $\lambda \sim W$ . For illustration, we chose a ribbon placed on a sinusoidally shaped substrate,  $h(x) = A \sin(2\pi x/\lambda)$  with  $A = 20 \text{ nm}$  and  $\lambda = 20 \text{ nm}$ . This leads to an effective potential

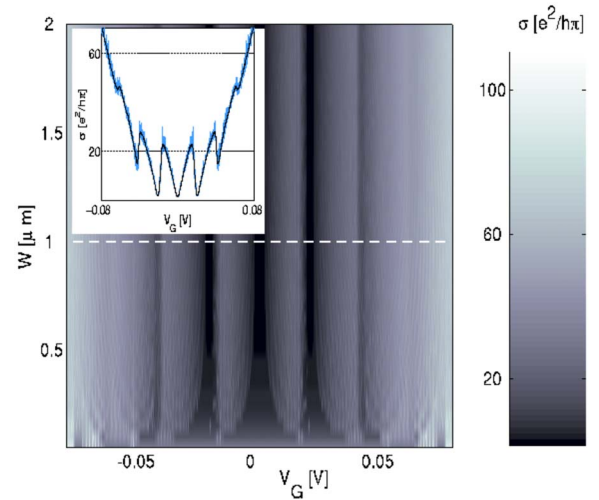


FIG. 3. (Color online) Conductivity ( $\sigma = GL/W$ ) for a graphene sheet of length  $L=1 \mu\text{m}$  with a periodic potential  $V_0 \sin(2\pi x/\lambda)$  ( $V_0 \sim 2.5 \text{ meV}$ ,  $\lambda=100 \text{ nm}$ ) as a function of gate voltage and sheet width  $W$ . The pseudogaps at  $V_G=0.02 \text{ eV}$  and  $V_G=0.04 \text{ eV}$  shown in Fig. 2 correspond to local minima in the conductivity. The inset shows the conductivity along the white dashed line ( $W=1 \mu\text{m}$ ) corresponding to the band diagram in Fig. 2. The thick line represents an average over nearby gate voltages, which removes the Fabry-Pérot interferences (see text). The nonaveraged data are shown as the thin (blue) line.

(see Fig. 4) of the order of 10 meV with an effective wavelength of the order of 80 nm (consistent with the assumption  $ka_0 \ll 1$ ). Choosing a width of  $W=100 \text{ nm}$  thus puts us in the desired regime. Figure 5 shows the conductance of a graphene ribbon with  $L=1 \mu\text{m}$  as a function of the backgate voltage (thick blue solid curve) calculated using the transfer matrix method described above. The conductance of a flat ribbon of equivalent length  $s(L)$  is also shown for comparison (red dashed curve). Both curves have been averaged over nearby points to remove spurious interferences arising from the abrupt boundary conditions. Nonaveraged data for the corrugated sheet are shown as the thin (blue) line.

A comparison of the conductances of flat and corrugated graphene sheets shown in Fig. 5 reveals two distinct features. Firstly, there is an asymmetry in the conductance of a corrugated sheet with respect to positive and negative backgate voltages because the average effective potential  $\bar{\Phi}_{\text{eff}}$  is strictly positive. This results in a total shift  $\Delta V_G = \bar{\Phi}_{\text{eff}}$  as well as in changes in the detailed structure. Secondly, the effect of corrugation is clearly seen to strongly alter the conductance

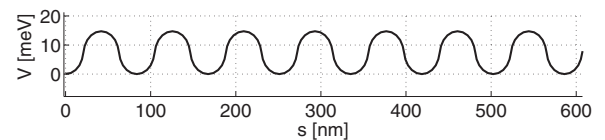


FIG. 4. Effective potential along a graphene sheet of shape defined by  $h(x) = A \sin(2\pi x/\lambda)$ ;  $A = 20 \text{ nm}$  and  $\lambda = 20 \text{ nm}$ .

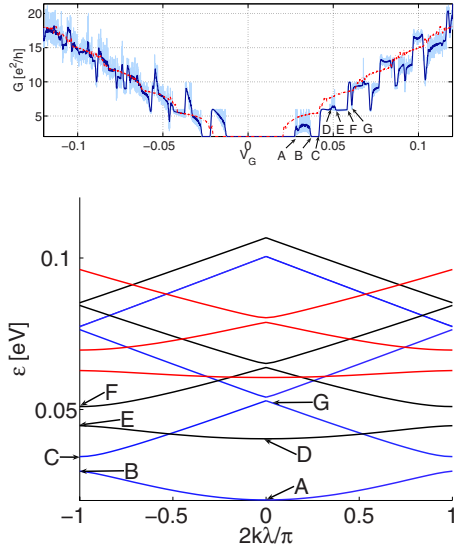


FIG. 5. (Color online) Conductance of a graphene ribbon as a function of gate voltage (left panel). The conductance of a ribbon placed on a corrugated surface (thick blue solid curve) is asymmetric with respect to the sign of the gate voltage in contrast to when the surface is flat (red dashed curve). The origin of this asymmetry is that the curvature-induced potential is not symmetric. Focusing on positive gate bias we can identify points (A–G) in the conductance curve, corresponding to switching on and off conductance in specific channels. The corresponding band edges for an infinite ribbon are shown in the right panel. For negative  $V_G$ , similar features appear in the conductance (not labeled).

due to conductance channels being switched on and off. This can be traced to the band structure for an infinite system with the corresponding parameters shown in the right panel of Fig. 5 (N.B.: the unaffected  $n=0$  band has been omitted).

Finally, we have also considered short graphene ribbons where  $L \sim W \sim \lambda$ . Figure 6 shows the conductance of a ribbon with  $s(L) \approx 160$  nm, and therefore only two potential maxima (double barrier). Again, comparing with a flat system of equal length, we find that the overall features in the conductance change in the same qualitative ways as described above. In this case, however, one should be careful not to confuse structure in the conductance due to the Fabry-Pérot-like interferences, on the one hand, with structure due to resonant tunneling, on the other. In this case, both effects are of similar importance.

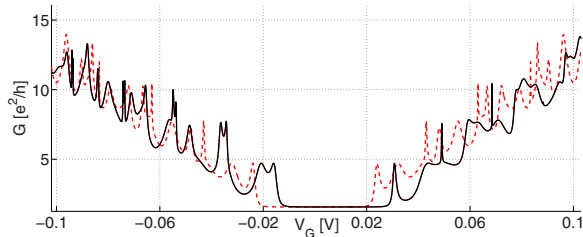


FIG. 6. (Color online) Conductance of a short metallic ribbon with (solid, black) and without (dashed, red) corrugation.

## IV. CONCLUSIONS

In conclusion, we have shown that placing graphene on an artificially corrugated surface produces an effective local potential for the graphene electrons. This potential, which is related to the local curvature, can be tailored to significantly alter the transport properties of graphene. Specifically we have considered the effect on the electrical conductance of periodic potentials and showed how the band structure manifests itself in graphene nanoribbons. Such a relation between transport properties and geometrical configurations may add to the number of design degrees of freedom available for constructing graphene-based electronic devices. It may also provide an alternative transduction mechanism in graphene-based NEMS.

## ACKNOWLEDGMENTS

We are grateful for stimulating discussions with Leonid Gorelik. Funding was provided by the Swedish Foundation for Strategic Research (SSF) and the Swedish Research Council (VR).

## APPENDIX: EFFECTIVE POTENTIAL

Here, we derive the effective Dirac Hamiltonian and the form of the curvature-induced effective potential used in this paper. We use the following tight binding Hamiltonian for noninteracting electrons in the  $\pi$  orbitals of graphene:

$$H = \sum_{\substack{i \in A \\ j \in B}} t_{ij} (a_i^\dagger b_j + b_j^\dagger a_i) + \sum_{\substack{i \in A \\ j \in A}} t'_{ij} (a_i^\dagger a_j + a_j^\dagger a_i) \\ + \sum_{\substack{i \in B \\ j \in B}} t'_{ij} (b_i^\dagger b_j + b_j^\dagger b_i) + \sum_{i \in A} \epsilon_i a_i^\dagger a_i + \sum_{i \in B} \epsilon_i b_i^\dagger b_i.$$

Here,  $A$  and  $B$  denote the respective sublattices. The  $A$  sites are related by the fundamental lattice vectors  $\mathbf{a}_1 = (0, \sqrt{3})a_0$  and  $\mathbf{a}_2 = \frac{1}{2}(3, \sqrt{3})a_0$ , where  $a_0$  is the in-plane interatomic spacing. We also define  $\mathbf{a}_0 = \frac{1}{2}(3, -\sqrt{3})a_0$ . The vectors connecting the  $A$  sites to the  $B$  sites are  $\mathbf{b}_1 = (1, 0)a_0$ ,  $\mathbf{b}_2 = \frac{1}{2}(-1, \sqrt{3})a_0$ , and  $\mathbf{b}_3 = \frac{1}{2}(-1, -\sqrt{3})a_0$ . Due to deformation of the sheet, the matrix elements  $t_{ij}$  and  $t'_{ij}$  will not be constant throughout the lattice but will fluctuate depending on the local shape. In this appendix, we will write these matrix elements as  $t_{ij} = t + \delta t_{\mathbf{b}_j}(\mathbf{r}_i)$  and  $t'_{ij} = t' + \delta t'_{\mathbf{a}_j}(\mathbf{r}_i)$ , respectively. By expanding around the Fermi points ( $\mathbf{K}, \mathbf{K}'$ ), one finds a low energy effective Dirac Hamiltonian

$$H = \int d^2\mathbf{r} \Psi^\dagger(\mathbf{r}) \mathcal{H}(\mathbf{r}) \Psi(\mathbf{r}),$$

where

$$\mathcal{H} = \begin{bmatrix} \sigma \cdot [-iv_F \nabla + \mathbf{A}(\mathbf{r})] & 0 \\ 0 & \sigma^T \cdot [-iv_F \nabla + \mathbf{A}(\mathbf{r})] \end{bmatrix} + V(\mathbf{r}).$$

Here, we have defined  $\sigma = \sigma_x \hat{x} + \sigma_y \hat{y}$ ,  $\sigma^T = \sigma_x \hat{x} - \sigma_y \hat{y}$ , and  $v_F = 3ta_0/2$ . The effective vector potential is  $\mathbf{A}(\mathbf{r}) = \hat{x} \text{Re } \mathcal{A}(\mathbf{r})$

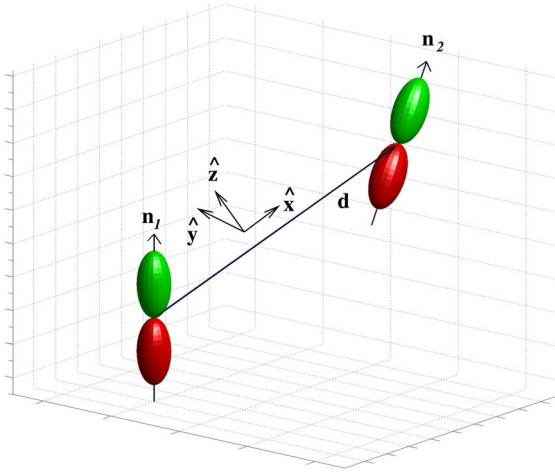


FIG. 7. (Color online) Illustration of the local coordinates used for evaluating the hopping matrix elements.

$-\hat{y} \text{Im } \mathcal{A}(\mathbf{r})$  where,  $\mathcal{A}(\mathbf{r}) \equiv [\sum_{j=1}^3 \delta t_{\mathbf{b}_j}(\mathbf{r}) e^{i\mathbf{K} \cdot (\mathbf{b}_j - \mathbf{b}_1)}]$ . We write the on-site potentials as  $V(\mathbf{r}) = [\epsilon(\mathbf{r}) - 3t' + \Phi_{\text{eff}}(\mathbf{r})]$ . Here,  $\epsilon(\mathbf{r}_i) = \epsilon_i$  and

$$\Phi_{\text{eff}}(\mathbf{r}) \equiv 2 \sum_{j=0}^2 \delta t'_{\mathbf{a}_j}(\mathbf{r}) \cos(\mathbf{K} \cdot \mathbf{a}_j). \quad (\text{A1})$$

To find how  $\Phi_{\text{eff}}(\mathbf{r})$  arises due to curvature, we consider the change of next nearest neighbor hopping. To find an explicit expression in terms of the shape of the graphene sheet, we first consider the hopping matrix element between two  $\pi$  orbitals situated as in Fig. 7. We decompose the normal vectors  $\mathbf{n}_{1,2}$  into components of a local coordinate system with an  $x$  axis along the vector  $\mathbf{d} = d\hat{x}$  connecting two sites (see Fig. 7),

$$\mathbf{n}_{1,2} = n_{1,2}^{(x)} \hat{x} + n_{1,2}^{(y)} \hat{y} + n_{1,2}^{(z)} \hat{z}.$$

This results in the hopping matrix elements<sup>19</sup>

$$\begin{aligned} t' &= V_{pp\pi}^{(d)} (n_1^{(y)} n_2^{(y)} + n_1^{(z)} n_2^{(z)}) + V_{pp\sigma}^{(d)} n_1^{(x)} n_2^{(x)} \\ &= V_{pp\pi}^{(d)} \mathbf{n}_1 \cdot \mathbf{n}_2 + (V_{pp\sigma}^{(d)} - V_{pp\pi}^{(d)}) \frac{(\mathbf{n}_1 \cdot \mathbf{d})(\mathbf{n}_2 \cdot \mathbf{d})}{d^2} \\ &\approx \frac{d_0^2}{d^2} \left[ V_{pp\pi} \mathbf{n}_1 \cdot \mathbf{n}_2 + (V_{pp\sigma} - V_{pp\pi}) \frac{(\mathbf{n}_1 \cdot \mathbf{d})(\mathbf{n}_2 \cdot \mathbf{d})}{d^2} \right]. \end{aligned} \quad (\text{A2})$$

The prefactor  $(d_0/d)^2$  accounts for the deviations from the equilibrium distance  $d_0$  when the sheet is deformed,<sup>19</sup> i.e.,  $V_{ppx}^{(d)} \approx (d_0/d)^2 V_{ppx}$ . We consider now a flat graphene surface with an orthogonal coordinate system  $\mathbf{u} = (u_1, u_2)$  (see Fig. 8). The deformed surface has three-dimensional coordinates  $\mathbf{x} = (x, y, z)$ . The surface can be described by the Gauss equations<sup>26</sup>

$$\mathbf{x}_{kl} = \Gamma_{kl}^i \mathbf{x}_i + L_{kl} \mathbf{n}.$$

Here,  $\mathbf{n}$  is the surface normal and the subscript notation  $x_k$   $k=1,2$  denotes differentiation with respect to  $u_k$ , i.e.,  $\mathbf{x}_k$

$$\mathbf{x}(\mathbf{u}) = (x(u_1, u_2), y(u_1, u_2), z(u_1, u_2))$$

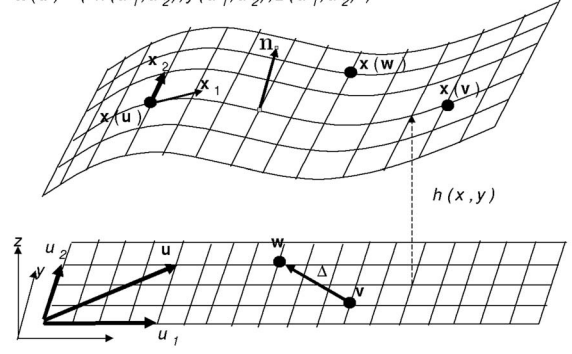


FIG. 8. Mapping from undeformed to deformed surface and notation used in the derivation of corrections arising from curvature.

$= \frac{\partial \mathbf{x}}{\partial u_k}$ . Repeated indices are summed over. In this paper, we consider only graphene which is deformed without any stretching. The surface is thus isometric to the plane configuration. In this case, all Christoffel symbols  $\Gamma_{kl}^i$  are identically zero and the Gauss equations reduce to  $\mathbf{x}_{kl} = L_{kl} \mathbf{n}$ . Together with the Weingarten equations

$$\frac{\partial \mathbf{n}}{\partial u_k} = -L_{kl} \mathbf{x}_l,$$

the graphene surface is completely described. We can now find expressions for the quantities appearing in Eq. (A2). For this purpose, consider two points  $\mathbf{v}$  and  $\mathbf{w}$  on the undeformed surface and define  $\Delta = (\mathbf{w} - \mathbf{v})$  (see Fig. 8). By expanding to lowest nonvanishing order in  $L_{kl}$  and using the Gauss-Weingarten equations, we find

$$\mathbf{n}(\mathbf{v}) \cdot \mathbf{n}(\mathbf{w}) \approx 1 - \frac{1}{2} \Delta_k \Delta_l L_{kn} L_{ln},$$

$$d^2 \approx d_0^2 - \frac{1}{12} \Delta_k \Delta_l \Delta_m \Delta_n L_{kl} L_{mn},$$

$$[\mathbf{n}(\mathbf{w}) \cdot \mathbf{d}][\mathbf{n}(\mathbf{v}) \cdot \mathbf{d}] \approx -\frac{1}{4} \Delta_k \Delta_l \Delta_m \Delta_n L_{kl} L_{mn}.$$

By inserting these into Eq. (A2), we obtain

$$\begin{aligned} t'_{12} &= V_{pp\pi} \left( 1 - \frac{1}{2} \Delta_k \Delta_l L_{kn} L_{ln} + \frac{1}{3} \frac{\Delta_k \Delta_l \Delta_m \Delta_n L_{kl} L_{mn}}{\Delta_j \Delta_j} \right) \\ &\quad - V_{pp\sigma} \frac{1}{4} \frac{\Delta_k \Delta_l \Delta_m \Delta_n L_{kl} L_{mn}}{\Delta_j \Delta_j} \frac{\Delta_1^2}{\Delta_j \Delta_j}. \end{aligned}$$

If bending is only in the  $x$  direction (Fig. 8), we have  $L_{kl} = \delta_{k1} \delta_{l1} (\partial_x^2 h)$ , which leads to

$$\tilde{t}' = t' - \frac{1}{2} (\partial_x^2 h)^2 \Delta_1^2 \left[ \left( 1 - \frac{2}{3} \frac{\Delta_1^2}{\Delta_j \Delta_j} \right) V_{pp\pi} + \frac{1}{2} \frac{\Delta_1^2}{\Delta_j \Delta_j} V_{pp\sigma} \right].$$

To find  $\Phi_{\text{eff}}$ , we need  $\delta t'_{\mathbf{a}_j} = \tilde{t}'_{\mathbf{a}_j} - t'$ . Evaluation is straightforward and we find

$$\delta t'_{\mathbf{a}_1} = 0,$$

$$\begin{aligned} \delta t'_{\mathbf{a}_0} &= \delta t'_{\mathbf{a}_2} \\ &= -(\partial_x^2 h)^2 \frac{9}{8} a^2 \left[ -\frac{1}{2} V_{pp\pi} + \frac{9}{8} V_{pp\sigma} \right]. \end{aligned}$$

Thus, the effective potential is given by

$$\begin{aligned} \Phi_{\text{eff}}(\mathbf{r}) &\equiv 2 \sum_{j=0}^2 \delta t'_{\mathbf{a}_j}(\mathbf{r}) \cos(\mathbf{K} \cdot \mathbf{a}_j) \\ &= \frac{27}{4} a_0^2 (\partial_x^2 h)^2 \left( \frac{3}{8} V_{pp\sigma} - \frac{1}{6} V_{pp\pi} \right). \end{aligned}$$

Rehybridization of the nearest neighbor orbital also leads to an effective potential with the same sign and of the same order of magnitude.<sup>16</sup> To fully analyze the true effective potential, one has to do first principle calculations. For the purpose of this work, this is not crucial and we are satisfied with an order of magnitude estimate of the potential.

\*andreas.isacsson@chalmers.se

<sup>1</sup>K. S. Novoselov, A. K. Geim, S. V. Morozov, D. Jiang, Y. Zhang, S. V. Dubonos, I. V. Grigorieva, and A. A. Firsov, *Science* **306**, 666 (2004).

<sup>2</sup>K. S. Novoselov, A. K. Geim, S. V. Morozov, D. Jiang, M. I. Katsnelson, I. V. Grigorieva, S. V. Dubonos, and A. A. Firsov, *Nature (London)* **438**, 197 (2005).

<sup>3</sup>Y. Zhang, Y.-W. Tan, H. L. Stormer, and P. Kim, *Nature (London)* **438**, 202 (2005).

<sup>4</sup>K. Nomura and A. H. MacDonald, *Phys. Rev. Lett.* **98**, 076602 (2007).

<sup>5</sup>J. Tworzydło, B. Trauzettel, M. Titov, A. Rycerz, and C. W. J. Beenakker, *Phys. Rev. Lett.* **96**, 246802 (2006).

<sup>6</sup>A. K. Geim and K. S. Novoselov, *Nat. Mater.* **6**, 183 (2007).

<sup>7</sup>M. Katsnelson and K. Novoselov, *Solid State Commun.* **143**, 3 (2007).

<sup>8</sup>A. L. Vazquez de Parga, F. Calleja, B. Borca, M. C. G. Passeggi, Jr., J. J. Hinarejos, F. Guinea, and R. Miranda, arXiv:0709.0360 (unpublished).

<sup>9</sup>V. P. Gusynin and S. G. Sharapov, *Phys. Rev. Lett.* **95**, 146801 (2005).

<sup>10</sup>N. M. R. Peres, F. Guinea, and A. H. Castro Neto, *Phys. Rev. B* **73**, 125411 (2006).

<sup>11</sup>V. V. Cheianov and V. I. Fal'ko, *Phys. Rev. B* **74**, 041403(R) (2006).

<sup>12</sup>V. V. Cheianov, V. Fal'ko, and B. L. Altshuler, *Science* **315**, 1252 (2007).

<sup>13</sup>Z. Xu, Q.-S. Zheng, and G. Chen, *Appl. Phys. Lett.* **90**, 223115 (2007).

<sup>14</sup>J. S. Bunch, A. M. van der Zande, S. S. Verbridge, I. W. Frank, D. M. Tanenbaum, J. M. Parpia, H. G. Craighead, and P. L. McEuen, *Science* **315**, 490 (2007).

<sup>15</sup>A. H. Castro Neto, F. Guinea, N. M. R. Peres, K. S. Novoselov, and A. K. Geim, arXiv:0709.1163 (unpublished).

<sup>16</sup>A. H. Castro Neto and E.-A. Kim, arXiv:cond-mat/0702562 (unpublished).

<sup>17</sup>F. Guinea, M. I. Katsnelson, and M. A. H. Vozmediano, arXiv:0707.0682 (unpublished).

<sup>18</sup>T. O. Wehling, A. V. Balatsky, M. I. Katsnelson, and A. I. Lichtenstein, arXiv:0710.5828 (unpublished).

<sup>19</sup>W. A. Harrison, *Elementary Electronic Structure*, revised ed. (World Scientific, Singapore, 2004).

<sup>20</sup>L. Brey and H. A. Fertig, *Phys. Rev. B* **73**, 235411 (2006).

<sup>21</sup>C. L. Roy, B. Mendez, and F. Dominguez-Adame, *J. Phys. A* **27**, 3539 (1994).

<sup>22</sup>B. F. Samsonov, A. A. Pecheritsin, E. O. Pozdeeva, and M. L. Glasser, *Eur. J. Phys.* **24**, 435 (2003).

<sup>23</sup>A. Calogeracos and N. Dombey, *Contemp. Phys.* **40**, 313 (1999).

<sup>24</sup>S. Datta, *Electronic Transport in Mesoscopic Systems* (Cambridge University Press, Cambridge, 1995).

<sup>25</sup>M. Katsnelson, *Eur. Phys. J. B* **57**, 225 (2007).

<sup>26</sup>D. J. Struik, *Lectures on Classical Differential Geometry*, 2nd ed. (Dover, New York, 1988).